ELSEVIER

Polymer 41 (2000) 7175–7192

polymer

The influence of molecular weight and thermal history on the thermal, rheological, and mechanical properties of metallocene-catalyzed linear polyethylenes

K. Jordens[1,a], G.L. Wilkes[a,*], J. Janzen[b], D.C. Rohlfing[b], M.B. Welch[b]

[a]*Polymer Materials and Interfaces Laboratory, Department of Chemical Engineering, Virginia Polytechnic Institute and State University, Blacksburg, VA 24061, USA*

[b]*Phillips Petroleum Company Research Center, Bartlesville, OK 74004, USA*

Received 4 May 1999; received in revised form 9 December 1999; accepted 29 December 1999

Abstract

Several linear polyethylene homopolymers of varied molecular weight ($13 \leq \bar{M}_w \leq 839$ kg/mol) were synthesized with a metallocene catalyst and characterized. The synthetic approach resulted in relatively narrow molecular weight distributions ($2.3 < \bar{M}_w/\bar{M}_n < 3.6$) as measured by size exclusion chromatography. The melt rheological data, $|\eta^*(\omega)|$ were modeled by the Carreau–Yasuda equation. The as-polymerized polymer fluffs were compression molded into films of quenched and slowly cooled thermal treatments. This resulted in a range of sample densities between 0.9302 and 0.9800 g/cm^3, due to variations in the crystal content. The thermal, morphological, and mechanical behaviors were examined for the dependencies on both molecular weight and thermal treatment. The small-strain tensile deformation properties, Young's modulus, yield stress, and yield strain, were directly related to percent crystallinity, independent of molecular weight. However, increasing molecular weight led to a suppression of the peak in the stress–strain curves at the yield point. The large-strain deformation properties, toughness and strain at break, were influenced by the competing effects of percent crystallinity and molecular weight. The slit-smeared long spacings increased with molecular weight. There was a progression from ridged and planar lamellae to curved C and S-shaped lamellae with increasing molecular weight. Thermal treatment had a large influence on the shape of the mechanical α-relaxation, while the crystal content affected the magnitudes of the mechanical γ and β-relaxations.

Keywords: Polyethylene; Metallocene; Mechanical properties

1. Introduction

Metallocene catalysis allows polyolefins of comparatively narrow molecular weight distribution to be produced. Under metallocene catalysis, polymer chain length is dependent on the relative rates of propagation versus the numerous possible termination reactions. Among the latter are chain transfer to ethylene (or other comonomer if applicable), chain transfer to metal alkyls, chain transfer to hydrogen, and β-hydride (β-H) elimination [1]. Since temperature has a different effect on each of these termination reactions as well as the propagation reaction, molecular weight is a function of the polymerization temperature. In fact, there is an inverse relationship between molecular weight and reaction temperature due to the relatively high rate of the β-H elimination reaction at high temperatures [2]. This terminating reaction leaves an unsaturated (vinyl) end group on the polymer chain. However, for polymerization at very low temperature (below −20°C), the β-H elimination reaction (as well as most of the other termination reactions) is generally so slow relative to propagation that the molecular weight becomes a function of only the polymerization time, in analogy with living polymerizations [3]. Besides varying the temperature, molecular weight can also be controlled through the addition of hydrogen as a chain transfer agent, similar to conventional heterogeneous Ziegler–Natta catalyzed olefin polymerization. However, metallocene catalyzed ethylene polymerizations are much more sensitive to hydrogen concentration than are conventional heterogeneous Ziegler–Natta polymerizations [4].

* Corresponding author. Tel.: +1-540-231-5498; fax: +1-540-231-9511.

E-mail address: gwilkes@vt.edu (G.L. Wilkes).

[1] Present address: Texas Eastman Division, Eastman Chemical Company, P.O. Box 7444, Longview, TX 75607-7444, USA.

0032-3861/00/$ - see front matter
PII: S0032-3861(00)00073-2

Since polyolefins made from metallocene catalyst systems are now commercially available, it is desirable to understand their structure–property relationships. While the molecular weight distributions of this series of polyethylenes is not as narrow as can be obtained by some other synthetic routes [2,5], the breadth indexes $\bar{M}_w/\bar{M}_n$ from 2.34 to 3.59 are distinctly less than those of polyethylenes produced from more traditional catalysts, such as heterogeneous Ziegler–Natta or Phillips chromium oxide systems.

It is our goal to examine the influence of molecular weight and thermal history on the properties of a series of unoriented metallocene-catalyzed linear polyethylene homopolymers. A major focus of our study is the tensile deformation properties which are critically important in determining the suitability of a material for a given application. Janzen and Register [6–8] have surveyed a large data set of deformation properties of both commercial and developmental polyethylenes. They examined the influence of density on such properties. Crist et al. [9] looked for effects of crystallinity and lamellar thickness on Young's modulus and yield stress for several fractionated linear polyethylenes with $\bar{M}_w$ between 32.1 and 199 kg/mol and a whole polymer of $\bar{M}_w = 52$ kg/mol, $\bar{M}_w/\bar{M}_n = 2.89$. Similarly, Kennedy et al. [10] examined fractionated linear polyethylenes with $\bar{M}_w$ ranging from 23.3 to 911 kg/mol, $\bar{M}_w/\bar{M}_n$ between 1.14 and 1.43, and whole polymers with $\bar{M}_w$ between 40 and 351 kg/mol, $\bar{M}_w/\bar{M}_n$ from 1.88 to 2.30. Related studies [11–14] were performed in the same laboratory on random (statistical is the preferred classification) ethylene copolymers. There the authors studied the effects of molecular weight and its distribution, as well as thermal treatment, on deformation behavior and ultimate mechanical properties of these polyolefins. An earlier study by Popli and Mandelkern [15] involved examining the influence of the structural and morphological factors on the mechanical properties of polyethylenes which included structural variations such as linear, branched, and copolymer formulations. In general, these materials had broad molecular weight distributions. The tensile deformation experiments discussed in this manuscript are similar to the previously mentioned studies, and direct comparisons will be made in the results and discussion section. However, there exist some distinct differences between laboratories in experimental procedures. A notable disparity is in methods of sample preparation. Test specimens of the polyethylenes studied by Janzen and Register [6] were prepared according to ASTM D1928. The compression-molded samples prepared by Crist et al. [9] were quenched in ice water. In the cited studies by Mandelkern and workers, the authors have applied a wider range of thermal treatments, which allowed them to span a broader window of crystallinities and morphologies for each polymer. These treatments involved quenching from the melt to −130°C, quenching to −78°C, quenching in boiling water, slowly cooling in air, and slowly cooling inside the hot press, without pressure [10]. Our preparations are less varied. Only two thermal treatments were applied for each material: quenching from the melt to room temperature and slowly cooling in the hot press. Details will be given in the next section. The mechanical behavior of our series is further probed with dynamic mechanical spectroscopy from −150°C (near the γ-relaxation for the frequencies explored in this study) through the α-relaxation and to nearly the melting point. The α, β, and γ-relaxations are examined with respect to the crystal content and thermal treatment for each sample.

To complement the results from the mechanical tests, various other characterization methods have been employed. Melting endotherms observed with differential scanning calorimetry provided information regarding the mass fraction of the crystalline phase for each sample. These results were compared to those obtained from density measurements. Details concerning the semicrystalline structure, for example the long spacing, were estimated from small angle X-ray scattering data. The morphological structure was further examined by transmission electron microscopy of chlorosulfonic acid-stained samples. Linear viscoelastic behavior was examined through melt-rheological measurements and correlation to solid state behavior is made where appropriate.

2. Experimental approach

The polyethylene series examined in this study was prepared using a catalyst system based on bis(*n*-butyl cyclopentadienyl) zirconium dichloride as described in US Patent 5,411,925 and in patent application EP 612,753. All polymerizations were conducted in an autoclave reactor, with no added comonomer. The reactor was first charged with the solid catalyst under an isobutane atmosphere and liquid isobutane was added. The system was then brought to near polymerization temperature, and hydrogen was added as a chain transfer agent, as appropriate, for controlling molecular weight. Ethylene monomer was then charged to the reactor, and the reactor pressure was held constant by continuous addition of ethylene during the polymerization process. The reaction was terminated after 1 h by rapid venting of the apparatus. The reactor was then opened and the dry polymer fluff was removed. The molecular weight of the samples was controlled by varying the reaction conditions. Reaction temperatures spanned the range of 60–100°C and pressures varied from 1.22 to 4.24 MPa.

Size exclusion chromatography (SEC or GPC) was used to determine the molecular weight distributions for the series. The instrument was a Waters 150 CV GPC equipped with two Styragel HT 6E mixed-bed columns. Trichlorobenzene flowing at a rate of 1.0 ml/min at 140°C was the solvent; the polymer concentration was 1.86 g/l. Stabilizer (0.5 g/l BHT) was added to each solution. The injection volume for each test was 220 μl. A broad-standard integral method of universal calibration was used, with Phillips Marlex® BHB 5003 as the standard. The parameters used

Table 1
Molecular weight results from SEC and melt-rheological parameters for the polyethylene series at 230°C

$\bar{M}_n$ (kg/mol)	$\bar{M}_w$ (kg/mol)	$\bar{M}_w/\bar{M}_n$	Carreau–Yasuda parameters			E_a (kJ/mol)
			η_0 (Pa s)	τ_η (s)	a	
4.1	13	3.24	–[a]	–[a]	–[a]	–[a]
5.2	14	2.74	6.14	3.82×10^{-5} [b]	0.422[b]	–[c]
7.1	26	3.59	26.7	1.44×10^{-4} [b]	0.602[b]	–[c]
16	37	2.34	135	4.00×10^{-8} [b]	0.215[b]	–[c]
18	51	2.83	364	9.68×10^{-4}	0.565	30.1
35	105	3.05	4200	2.13×10^{-3}	0.333	–[c]
45	160	3.54	1.22×10^{4}	0.0195	0.598	–[c]
67	165	2.45	1.72×10^{4}	0.0198	0.393	–[c]
79	267	3.4	1.44×10^{5}	0.198	0.323	–[c]
125	320	2.56	1.01×10^{5}	0.190	0.521	30.3
241	839	3.49	9.81×10^{5}	2.69	0.635	–[c]

[a] Not measured—insufficient viscosity.
[b] Values poorly determined by the available data (uncertainties much larger than parameter values).
[c] Not measured.

in the Mark–Houwink–Sakurada equation [16], $[\eta] = K(\bar{M}_v)^a$, were $K = 0.0395$ ml/g and $a = 0.76$.

The rheological characteristics of the as-polymerized fluffs were surveyed using small-strain oscillatory shear measurements performed on a Rheometrics RMS-800 parallel-plate instrument under a nitrogen atmosphere. The initial gap was set to 1.6 mm, and a compression-molded disk of the polymer was equilibrated in the plates at the desired start temperature before trimming and beginning the measurements.

For the remaining characterization methods, it was necessary to have samples in the form of films. These were made from the fluffs by thermal compression molding. An appropriate amount of powder was loaded into a picture-frame mold and brought into thermal contact with the plates of a hot press which were at 155°C (roughly 14° above the equilibrium melting temperature for polyethylene [17,18]). The sample was held at this condition for approximately 10 min to allow the powder to melt. Following this, pressure was slowly applied to the mold to force the polymer to flow out into the shape of the frame. After 10–15 min, pressure was released while still holding the sample at 155°C to minimize molecular orientation. Two distinct thermal histories were employed for the series of molecular weights studied. The first, referred to as *quenched*, was the result of removing the mold from the hot press and sandwiching it between two room temperature steel plates, roughly 1 cm thick. The second, designated as *slowly cooled*, was accomplished by leaving the mold in the hot press (again, only in thermal contact, without much pressure) and turning off the heaters. Cooling to room temperature took approximately 8 h by this route.

Differential scanning calorimetry (DSC) was performed on a Perkin–Elmer DSC 7, which was calibrated using indium and tin standards. DSC samples weighed between 5 and 11 mg each and a heating rate of 20 K/min was applied during each scan. Each scan represents a first heating of the prepared films. Densities were measured at room temperature with a density-gradient column using the technique described in ASTM D 1505.

Small angle X-ray scattering (SAXS) experiments were performed with nickel filtered, slit collimated CuKα radiation (1.542 Å) [19] produced by a Philips generator, model PW1729. A Kratky camera and a one-dimensional M. Braun position-sensitive detector were used to collect the scattered radiation. Absolute intensities were calibrated through the use of a working standard (Lupolen 1811M) [19]. SAXS data will be presented as the slit-smeared scattered intensity $I(s)$ versus the scattering vector $s \equiv (2/\lambda)\sin(\theta/2)$, where λ is the incident beam wavelength and θ the radial scattering angle.

The instrument used for transmission electron microscopy (TEM) was a Philips model 420T, operated at 100 kV. Samples were prepared by staining with chlorosulfonic acid [20,21] to greatly increase the electron density of the amorphous phase. This provides adequate contrast for viewing with TEM. Samples were completely immersed in chlorosulfonic acid for approximately 2 h at 60°C. They were then washed and allowed to dry before being microtomed. Good images were obtained with samples microtomed at room temperature. The resulting micrographs (to be presented) show darkened amorphous regions and lighter crystalline domains.

An Instron model 4400R equipped with a 1-kN tension load cell was employed for tensile testing. The cell was calibrated with an 8-kg standard (78.45 N), and ultimate loads never exceeded 140 N. All tensile tests were conducted at 20°C with a crosshead speed of 25.4 mm/min. Specimens were stamped out of the prepared films with a "dog-bone" die (gauge length approximately 10 mm, thickness approximately 0.4 mm). At least 10 specimens were tested for each condition, to obtain satisfactory statistics.

Strain was not determined rigorously, but rather was taken as the crosshead displacement divided by the original

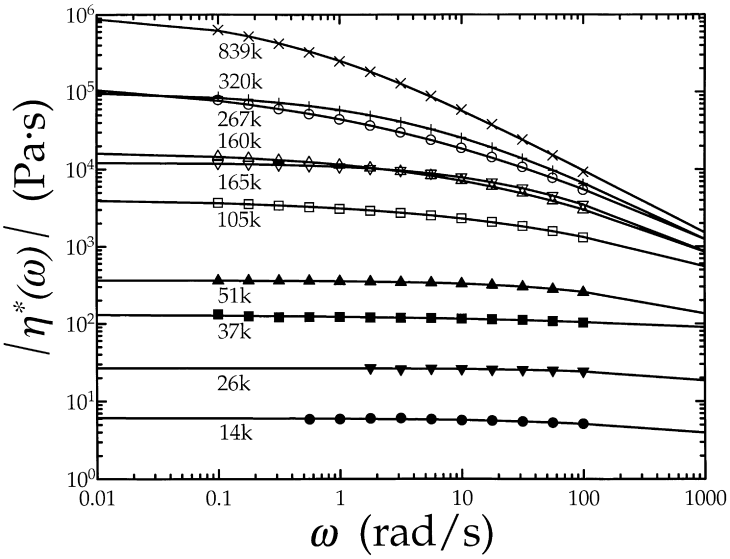

Fig. 1. Melt rheological behavior of the polyethylene series: $|\eta^*(\omega)|$ at 230°C. Drawn curves represent the Carreau–Yasuda equation fits of the data.

gauge length (10 mm). Therefore, values of Young's moduli are not absolute, but rather relative numbers which can be compared within the series.

Dynamic mechanical spectra were collected by a Seiko DMS 210 (also labeled DMA or DMTA by other manufacturers). Rectangular samples measured approximately $10 \times 4 \times 0.5\ mm^3$ ($\sim 2\ mm^2$ cross-sectional area being desirable for the instrument according to the manufacturer). The strain amplitude was set at 10 μm, which corresponds to 0.1% strain (well within the linear viscoelastic limit). The samples were loaded at room temperature and then quenched to −150°C with liquid nitrogen. The test was then started and data were collected for several frequencies from 0.1 to 10 Hz while ramping to approximately the near melting. Purified nitrogen was employed as a purge gas to prevent oxidation and degradation upon reaching elevated test temperatures. Slow heating rates (0.8–2.0 K/min) were used.

3. Results and discussion

3.1. Molecular weight

Molecular weight averages determined by SEC are listed in Table 1. $\bar{M}_w/\bar{M}_n$ ratios, indexes of relative breadths of the molecular weight distributions, range from 2.34 to 3.59. These are somewhat larger than the values around 2.0 that have been reported for some metallocene-catalyzed polyolefins, as mentioned above, but they still are quite small in comparison with the more common heterogeneous Ziegler–Natta catalyzed polyolefins, where they may be at least 4–8 [22], and distinctly less than for olefins produced with Phillips chromium oxide-type catalysts, for which the ratios often exceed 10.

Our polyethylene samples will be referred to below by their weight average molecular weights, $\bar{M}_w$, in units of kg/mol.

3.2. Melt rheology

Simple mathematical models formulated for representing steady-flow viscosity data (e.g. the Carreau–Yasuda, power law, Ellis, etc.), are often written in terms of shear rate. However, modern oscillatory rheometers monitor complex viscosity as a function of the oscillatory frequency, not steady-shear viscosity as a function of shear rate. A common method of translating between the two kinds of experimental data is to use the Cox–Merz rule [23] which is stated mathematically as follows:

$$\eta(\dot{\gamma}) = |\eta^*(\omega)|_{\omega = \dot{\gamma}}, \tag{1}$$

where $\eta(\dot{\gamma})$ is the shear rate dependent viscosity, with $\dot{\gamma}$ the steady-state shear rate in reciprocal seconds, and where $|\eta^*(\omega)|$ is the magnitude of the frequency dependent complex viscosity derived from dynamic oscillatory experiments, with ω the sinusoidal shearing frequency in radians per second. Sometimes $\eta(\dot{\gamma})$ and $|\eta^*(\omega)|$ disagree at large deformation rates (which are generally not obtainable in oscillatory rheometers). However, it is well known [24] that:

$$\lim_{\dot{\gamma}\to 0} \eta(\dot{\gamma}) = \lim_{\omega\to 0} |\eta^*(\omega)| = \eta_0, \tag{2}$$

where η_0 is called the zero-shear viscosity.

The Carreau–Yasuda model has the following form [24]:

$$\frac{\eta(\dot{\gamma}) - \eta_\infty}{\eta_0 - \eta_\infty} = [1 + (\tau_\eta \dot{\gamma})^a]^{(n-1)/a}, \tag{3}$$

where η_∞ is the infinite-shear-rate viscosity. τ_η is a characteristic viscous relaxation time (denoted as λ in Ref. [24]) that defines the location of the transition from Newtonian to

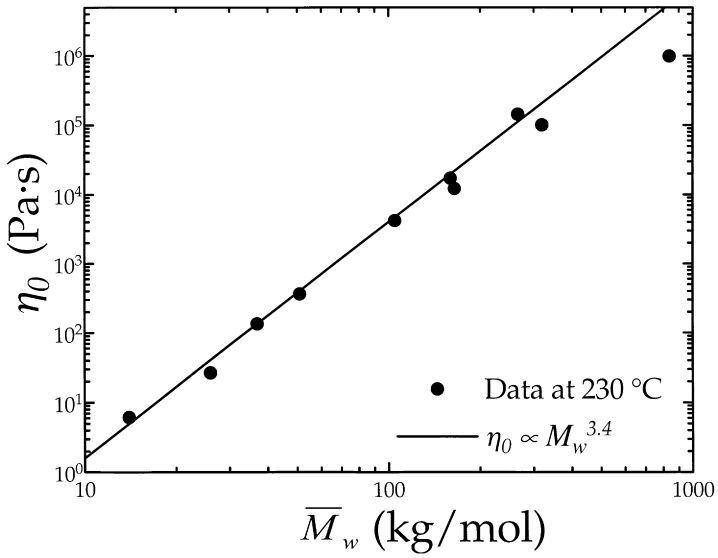

Fig. 2. Zero-shear viscosity (from the Carreau–Yasuda fits) at 230°C versus weight-average molecular weight for the polyethylene series.

shear-thinning behavior. In general τ_η is close to or slightly greater than the arithmetic mean time (first moment) of the terminal mode in the relaxation spectrum [25]. a is a dimensionless parameter (sometimes called "the Yasuda constant" since it was a parameter added to the Carreau equation by Yasuda) which describes the transition zone between the Newtonian plateau and the shear-thinning region and is inversely related to the breadth of this zone. [25,26] The exponent $(n-1)$ defines the slope of the $\eta(\dot{\gamma})$ versus $\dot{\gamma}$ curve within the power law region.

Graessley [27,28] presented a theory of polymer viscosity based on an entanglement concept in 1967. His development had the high-rate limiting slope of log η vs. log $\dot{\gamma}$ equal to $-9/11$. If we are to adopt this relationship in our Carreau–Yasuda model, then the quantity $(n-1)$ of Eq. (3) must be set equal to $-9/11$, or $n = 2/11$. This approach has proven useful [25] for fitting polyethylene melt viscoelasticity data. If n is used as an adjustable parameter, often Carreau–Yasuda parameter sets are inadequately determined by available data, and parameter comparisons among cases are not meaningful. A symptom of this is that parameter values are returned with error estimates much larger than the values themselves.

For our purposes, then, Eq. (3) is simplified by assuming that η_∞ is negligible (zero), setting n equal to 2/11, and employing the Cox–Merz rule. Then the Carreau–Yasuda model reduces to a form which we have employed for fitting the experimental rheology data:

$$|\eta^*(\omega)| = \eta_0[1 + (\tau_\eta\,\omega)^a]^{-(9/11)1/a}. \quad (4)$$

The rheological behavior of the 13 kg/mol polyethylene was unobtainable since this material had too low a viscosity to measure with the rheometer. For the remainder of the polyethylene series, the magnitude of the complex viscosity versus frequency data at 230°C are presented in Fig. 1. The continuous curves drawn in this figure are the Carreau–Yasuda equation fits of the experimental data and the parameter values derived from the fitting are displayed in Table 1. Since the materials of lower molecular weights display nearly Newtonian behavior across the entire experimental frequency range (for this temperature), the Carreau–Yasuda parameter η_0 is well determined but τ_η and a for these materials have large uncertainties. Indeed, the fitting procedure returned error estimates larger than the parameter values for the three lower molecular weights (14, 26, and 37 kg/mol). Hence it should be borne in mind that τ_η and a are not precisely determined for these three materials.

The zero-shear viscosity η_0 is plotted as a function of molecular weight in Fig. 2. Many linear polymers obey the empirical relationship $\eta_0 \propto (\bar{M}_w)^{3.4}$ above a critical molecular weight M_c, which is referred to [29,30] as the entanglement molecular weight (or the critical molecular weight for entanglement). The value of M_c for linear polyethylene is reported [31,32] as 3.8 kg/mol which is well below the molecular weight of all samples in our series. Hence the present materials are all entangled, and the data of Fig. 2 show an excellent fit to the 3.4-power law. Only for the highest molecular weight material, 839 kg/mol, is there a significant deviation.

The zero-shear viscosity generally follows Arrhenius temperature dependence above melting, that is, $\eta_0 \propto \exp(E_a/RT)$. Hence, a semilog plot of η_0 versus $1/T$ yields a line from which the melt flow activation energy E_a can be calculated from the slope. E_a is a measure of the temperature sensitivity of viscosity; small values imply little effect of temperature on the viscosity while large values imply strong dependence. For polyethylenes, the value of E_a is known to be a function of the chain topology. Values for *linear* polyethylene are reported between 25–30 kJ/mol [33–38].

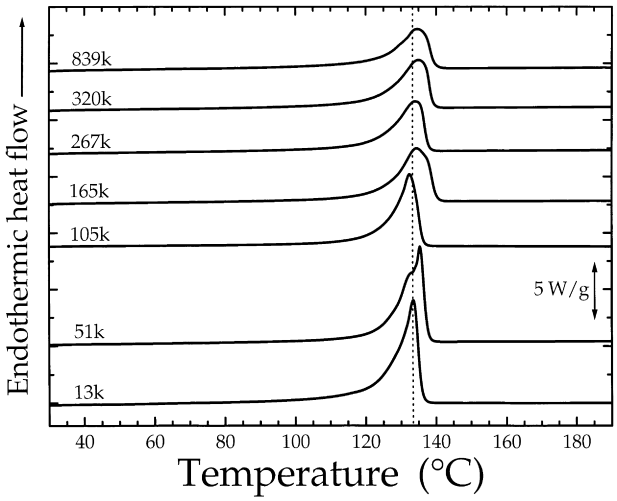

Fig. 3. DSC scans of the quenched polyethylene series. Traces are displaced vertically for clarity.

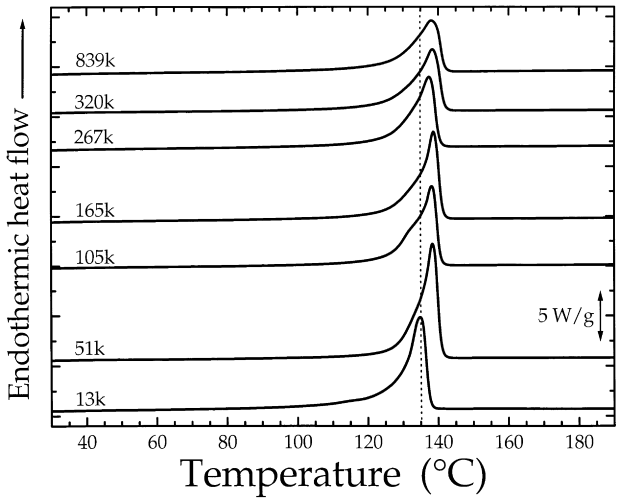

Fig. 4. DSC scans of the slowly cooled polyethylene series. Traces are displaced vertically for clarity.

Linear low-density polyethylene (LLDPE), which contains short-chain branching (SCB, where the side chains usually have 2–6 carbon members), has a reported [37,39,40] activation energy near 30 kJ/mol, and is generally a mild function of SCB content at low levels [41]. Isotactic polypropylene, which can be thought of as polyethylene with one methyl branch placed very regularly on every other backbone carbon,[2] has a melt flow activation energy of 39–43 kJ/mol [37,42,43]. Low-density polyethylene (LDPE) has many long chain branches (LCB), where such a branch is defined as being rheologically significant, i.e. its length exceeds the critical molecular weight for entanglement for the polymer, M_c. LDPE has a dramatically higher activation energy near 50 kJ/mol [37,44]. Other workers have reported [44] E_a as high as 167 kJ/mol for a long chain branched polyethylene containing 7.2 long chain branches per 10,000 backbone carbon atoms. This highly branched polymer sample was generated by gamma irradiation of high-density polyethylene (HDPE), which would likely produce some amount of SCB as well. Hence the presence of LCB has a significantly larger influence on the melt flow activation energy than SCB. From Table 1, the values of E_a for the 51 and 320 kg/mol samples are both approximately 30 kJ/mol. Since these two samples represent nearly the highest and lowest molecular weights of the series, it is anticipated that all the intermediate molecular weight samples also have similar values for the activation energy, and the observed values for the activation energy do not differ significantly from that (29.3 kJ/mol) reported by Arnett and Thomas [38] for strictly linear hydrogenated polybutadienes (model polyethylenes). From this and supporting evidence from DMS (to be discussed later), we conclude that LCB is essentially undetectable throughout the series. This conclusion is furthermore strongly confirmed by analysis of the data in Fig. 2 according to the scheme of Janzen and Colby [45].

[2] E_a is a function of tacticity for polypropylene. For i-PP and a-PP, E_a = 40 kJ/mol, but for s-PP, E_a = 50 kJ/mol [43].

3.3. Differential scanning calorimetry

The first-heating scans for the series of quenched polyethylene samples are shown in Fig. 3, and the corresponding scans of the slowly cooled samples in Fig. 4. Vertical displacements have been applied to successive scans for clarity. The dashed line of Fig. 3 at 133.6°C marks the peak of the melting endotherm for the 13 kg/mol sample, and is drawn to highlight the variation in the location of the melting points with molecular weight. Analogously, a dashed line is drawn in Fig. 4 at 135.0°C, the peak of the melting endotherm for the slowly cooled 13 kg/mol polyethylene material.

The melting endotherms of the higher molecular weight materials are broader than that of the lower molecular weight materials for both thermal treatments. The higher molecular weight polymers are kinetically limited to produce crystals of broader thickness distribution which leads to this observed endotherm broadening [18]. This can be attributed to the presence of a large number of entanglements for the higher molecular weight materials.

A crude calculation of the average number of entanglements per chain can be made by dividing the molecular weight of the polymer by the entanglement-spacing molecular weight, M_e. Generally M_e is determined from the plateau modulus, G_N^0, as follows [46–48]:

$$G_N^0 = \frac{4\rho RT}{5M_e}, \tag{5}$$

where ρ is the sample density at the absolute temperature T, and R is the universal gas constant. Using the data of Graessley and Edwards [31] (G_N^0 = 2.06 MPa, T = 463 K, ρ = 0.76 g/cm^3), one can calculate M_e = 1140 g/mol for

Table 2
Density, crystal mass fraction (w_c), and crystal volume fraction (ϕ_c) of the metallocene-catalyzed polyethylene series

$\bar{M}_w$ (kg/mol)	Thermal treatment	Density (g/cm^3)	w_c (DSC)	w_c (density)	ϕ_c (density)
13	Quenched	0.9714	0.84	0.79	0.76
	Slowly cooled	0.9800	0.87	0.83	0.81
51	Quenched	0.9568	0.72	0.70	0.66
	Slowly cooled	0.9699	0.82	0.78	0.75
105	Quenched	0.9461	0.61	0.64	0.60
	Slowly cooled	0.9604	0.73	0.72	0.69
165	Quenched	0.9432	0.61	0.62	0.58
	Slowly cooled	0.9563	0.73	0.70	0.66
267	Quenched	0.9403	0.56	0.60	0.56
	Slowly cooled	0.9517	0.68	0.67	0.63
320	Quenched	0.9367	0.58	0.58	0.54
	Slowly cooled	0.9484	0.65	0.65	0.61
839	Quenched	0.9302	0.52	0.54	0.49
	Slowly cooled	0.9439	0.62	0.62	0.58

linear polyethylene. More recently, Carrella et al. [49] have reported a value of $M_e = 830$ g/mol for polyethylene. Still another value can be estimated from a rule-of-thumb relation, namely $M_e = M_c/2$ to $M_c/3$. Considering the M_c value of 3800 g/mol mentioned earlier, this relation yields $M_e =$ 1300 to 1900 g/mol. Based on this range of values for M_e, it then follows that the 839 kg/mol sample has an average of between 441 and 1011 entanglements per chain, whereas the 13 kg/mol specimen has only between 7 and 16.

Tie molecules and the characteristics of the crystal–amorphous interface will also affect the melting behavior of macromolecules but the quantitative description of this effect is impossible without the knowledge of the molecular structure at the phase boundary [18].

Taking from the literature the heat of fusion of purely crystalline polyethylene to be 293 J/g (70 cal/g) [17,50,51], the crystal mass fraction (w_c) in each polyethylene sample is given by $w_c = \Delta H_m/293$ J/g, where ΔH_m is the measured heat of melting observed in the DSC scans. The results of this calculation are listed in Table 2. From this approach, crystallinities vary from 52% for the quenched 839 kg/mol sample to 87% for the slowly cooled, 13 kg/mol material. Clearly, for a given thermal treatment, increasing molecular weight leads to a decrease in the level of crystallinity. This has been observed in the past [52] and is a result of the reduction in the rate of crystallization with increasing molecular weight due to entanglement and viscosity effects.

3.4. Density measurements

Room-temperature densities for the series, as determined by the density gradient method, are listed in Table 2. Percent crystallinity values were calculated using the measured densities to complement those derived calorimetrically. Assuming a two-phase system composed of an amorphous

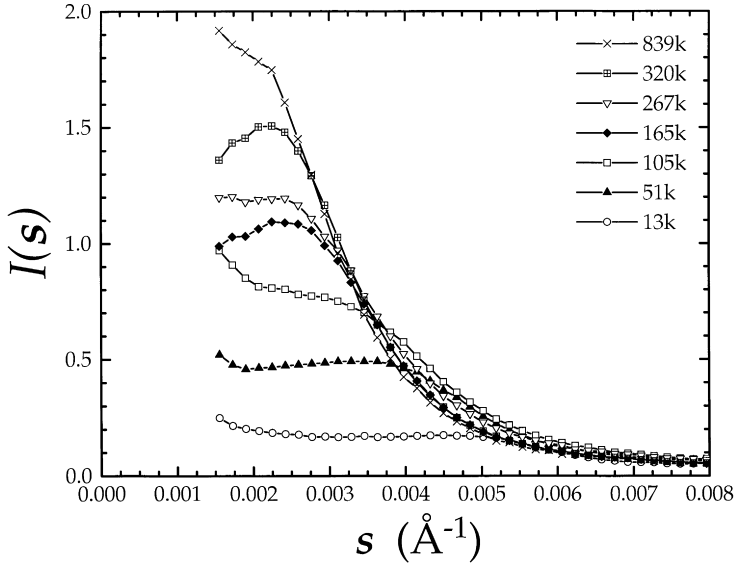

Fig. 5. Slit-smeared SAXS profiles for quenched polyethylenes.

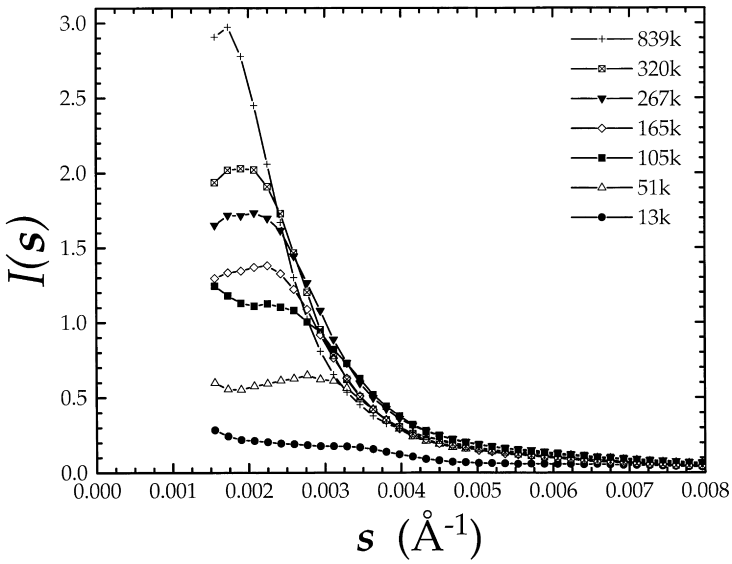

Fig. 6. Slit-smeared SAXS profiles for slowly cooled polyethylenes.

phase of density [7] $\rho_{am} = 0.852$ g/cm^3 and a crystalline phase of density [53] $\rho_c = 1.010$ g/cm^3, both the crystal volume fraction (ϕ_c) and crystal mass fraction (w_c) can be calculated through the following relations [19]:

$$\phi_c = \frac{\rho - \rho_{am}}{\rho_c - \rho_{am}} \quad \text{and} \quad w_c = \phi_c \frac{\rho_c}{\rho}. \tag{6}$$

Values of w_c for the series vary from 54% for the quenched 839 kg/mol sample to 83% for the slowly cooled 13 kg/mol material. Percent crystallinities determined from the density are, in general, in good agreement with those ascertained calorimetrically as seen in Table 2. Values of w_c calculated from the density will be used for the presentation of data throughout this report. This is an arbitrary choice since density and DSC yield similar values.

3.5. Small angle X-ray scattering behavior

Fig. 5 shows $I(s)$ vs. s for the quenched series and Fig. 6 for the slowly cooled series. Most of the curves show a characteristic interference peak, associated with a correlation length present in the samples. This correlation length corresponds to the long spacing, which is a combination of one lamellar thickness (ℓ_c) and one amorphous layer thickness (ℓ_{am}) for an ideal stacked lamellar structure. For both the quenched and slowly cooled series, the interference peaks shift to smaller angles (and hence the long spacings increase) with increasing molecular weight. Rault and Robelin-Souffaché [54] have plotted the long spacing versus the square root of molecular weight for various linear polyethylenes. They observed that cooling from the melt at 2 to 10 K/min, and rapid quenching all led to nearly identical slopes in this plot. The increase in the long spacing observed for the materials in the present study could be due to an increase in ℓ_c or an increase in ℓ_{am}, or both. From the TEM results to be discussed in the next section, it is ℓ_c that increases with molecular weight.

For a given molecular weight, the slowly cooled material has a larger long spacing than the quenched material. This is primarily due to a difference in ℓ_c, being larger for the slowly cooled material. The slowly cooled samples have larger ℓ_c because they were effectively crystallized at a smaller undercooling (also called the supercooling). The average initial lamellar thickness (ℓ_g^*, derived from the Lauritzen–Hoffman [55] model of crystal growth for flexible chains) is expected to be related to the undercooling $\Delta T = T_m - T_c$ as:

$$\ell_g^* \propto 1/\Delta T \tag{7}$$

Hence the closer to the melting temperature (T_m) that a polymer is crystallized (T_c), the thicker will be the average lamella.

3.6. Transmission electron microscopy

TEM was used to look at the morphological structures in the polyethylene series. A few selected micrographs are shown in Fig. 7(A)–(E). Sharper contrast was generally noted for slowly cooled samples compared to their quenched counterparts. This is due to the sharper separation of the crystalline and amorphous phases (and smaller interphase) in the slowly cooled samples compared to quenched samples of the same molecular weight. For the quenched set, the lack of this sharp separation leads to a more "fuzzy" or less defined lamellar texture. All samples probed by TEM (quenched and slowly cooled 13, 51, 267, and 839 kg/mol materials, although not all are shown) possessed stacked lamellar structures. No supermolecular structure is obvious in the micrographs although in two cases, structures resembling spherulites are observed (see Fig. 8).

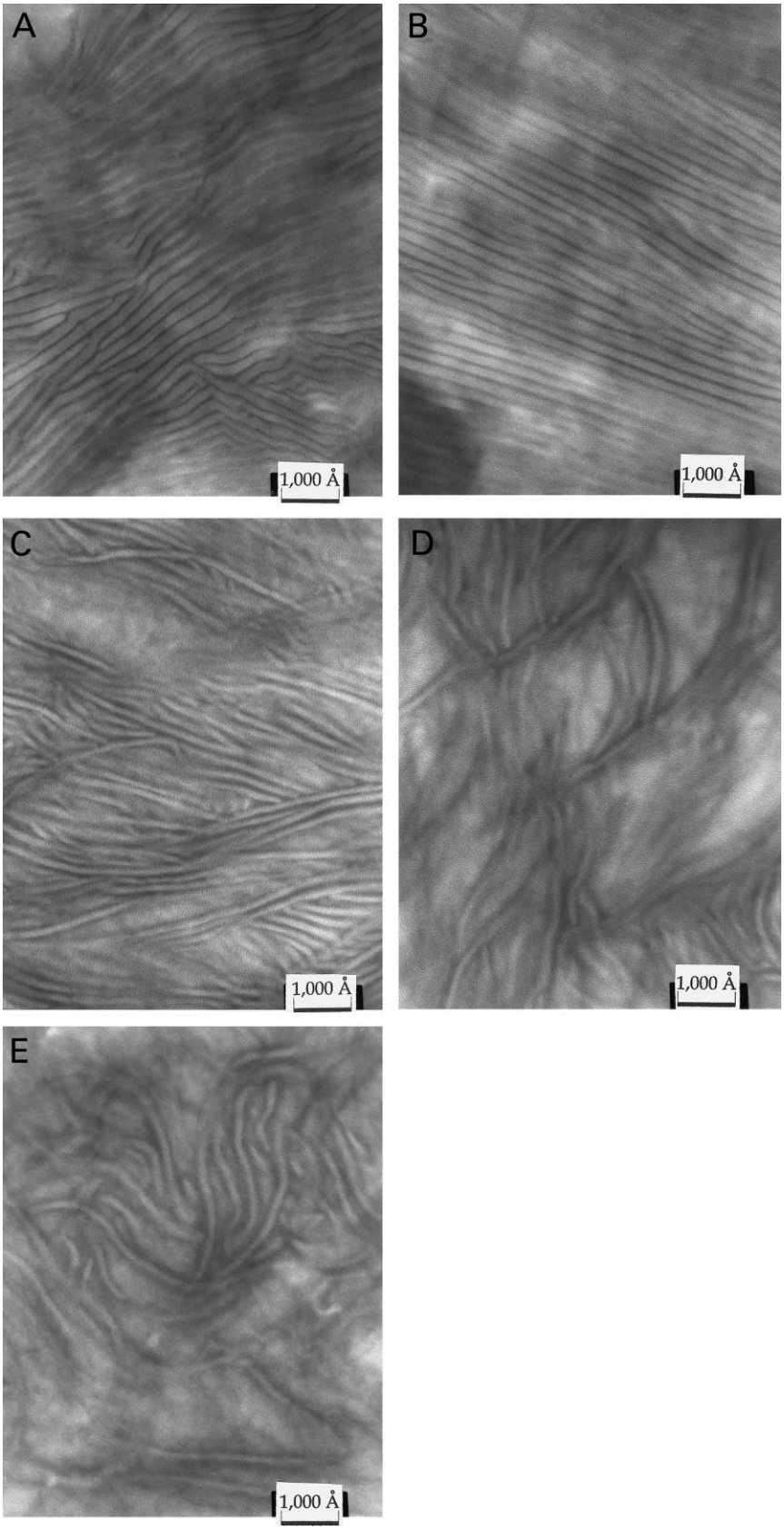

Fig. 7. Transmission electron micrographs: (A) 13 kg/mol slowly cooled; (B) 51 kg/mol slowly cooled; (C) 51 kg/mol quenched; (D) 267 kg/mol quenched; (E) 839 kg/mol quenched. All micrographs are at the same magnification.

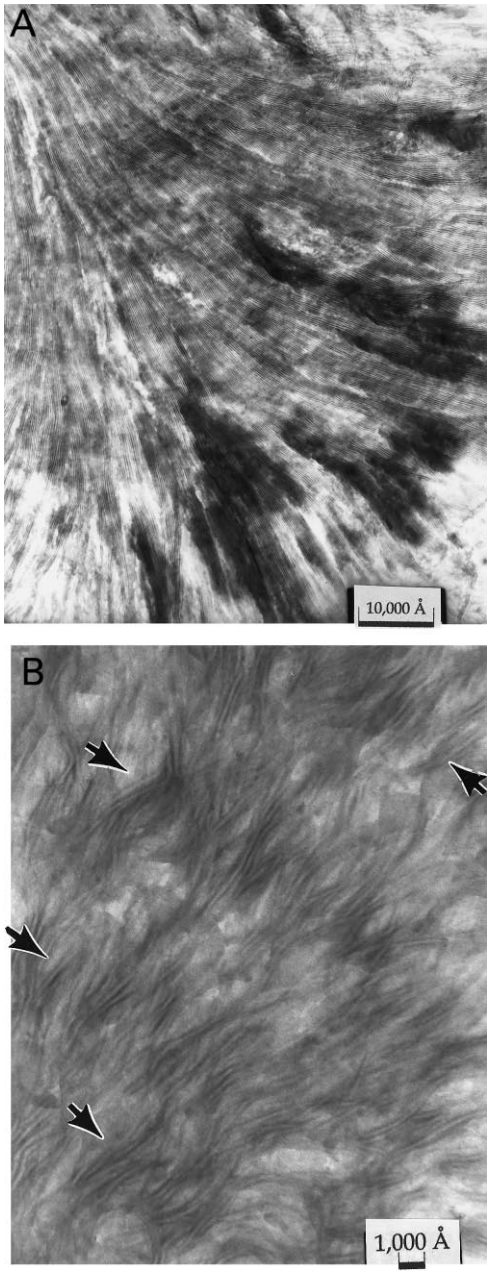

Fig. 8. Transmission electron micrographs which displayed spherulite-like superstructures: (A) 51 kg/mol slowly cooled (same sample as Fig. 7(B)); (B) 267 kg/mol quenched (same sample as Fig. 7 (D)). Arrows indicate areas where optical banding would occur under the polarized optical microscope.

Polyethylene of 13 kg/mol molecular weight displayed very long lamellae that remained fairly straight in the lateral direction. To follow existing terminology [56–58], the lamellae of the quenched 13 kg/mol material (not shown) were mostly *planar*, but some appeared curved. These lamellae were only slightly curved over their long reaching lengths, which were generally in excess of 1 μm. The slowly cooled 13 kg/mol sample had both planar and *ridged* lamellae, as seen in Fig. 7(A). The adjacent planar and ridged lamellae of this micrograph lie parallel (near the bottom, center of micrograph), suggesting a common crystallography as reported by Bassett and Hodge [56]. The average thickness of lamellae in the 13 kg/mol materials is greater for the slowly cooled sample (≈ 180 Å) compared to the quenched (not shown, however ≈ 100 Å), as expected from the undercooling argument of Eq. (7).

The 51 kg/mol slowly cooled material in Fig. 7(B) displays planar lamellae in a few areas, although the majority are curved. The curvature can be better observed in the lower magnification micrograph in Fig. 8(A). In this picture, a structure that resembles part of a spherulite (reminiscent of Fig. 4 of Bassett and Hodge [56]) can be observed, where the lamellae run fairly straight through the superstructure with slight splaying outward. Well-defined spherulites were not easily seen at lower magnifications (not shown). The lamellae of the slowly cooled 51 kg/mol material of Fig. 7(B) were thicker (≈ 160 Å) than the mostly curved lamellae seen in the quenched material (≈ 100 Å) of Fig. 7(C). For this quenched material, some C and S-shaped [56–59] lamellae were observed.

For the 267 kg/mol molecular weight materials, a clear transformation to dominant C and S shapes was observed for both thermal treatments. The quenched material is shown in Fig. 7(D). The slowly cooled 267 kg/mol sample (not shown) displayed irregular curved lamellae, roughly of C and S shapes. A lower magnification micrograph of the quenched 267 kg/mol material is shown in Fig. 8(B). This picture shows perhaps part of a spherulite which would display optical banding [59]. Optical banding occurs due to spiraling of the *c*-axis (chain axis) about the *b*-axis while traveling along the radial direction of the spherulite [58,60–63]. Four "bands" can be discerned in the image.

Both thermal treatments for the 839 kg/mol polyethylene exhibited large curvature of relatively short lamellae. Many C and S-shaped lamellae were visible, as shown for the quenched material in Fig. 7(E). The slowly cooled material (not shown) had some of the thickest lamellae of the series, which were on the order of 240 Å, and were slightly longer than the lamellae of the quenched sample.

Generally speaking, the low molecular weight samples possessed very long, fairly straight (in the lateral direction), lamellae. They were mostly planar, with some areas appearing ridged in nature. Increasing the molecular weight led to shorter, more curved lamellae. Curved lamellae progressed into C and S shapes. Curving has been suggested [56] to be due to deformation during growth predominantly by shear forces, which are present under régime II crystallization conditions. These changes in morphology, primarily due to molecular weight, are illustrated by the series of micrographs in Fig. 7(A)–(E). Such a transformation has been similarly observed by Bassett and coworkers [56–58] and others [64,65]. Fractionated polyethylenes of molecular weights 5.6, 11, 46, and 195 kg/mol, quenched from the melt, have been observed to transform similarly from long, planar, straight lamellae to short, curved lamellae in the work of Voigt-Martin and Mandelkern [65].

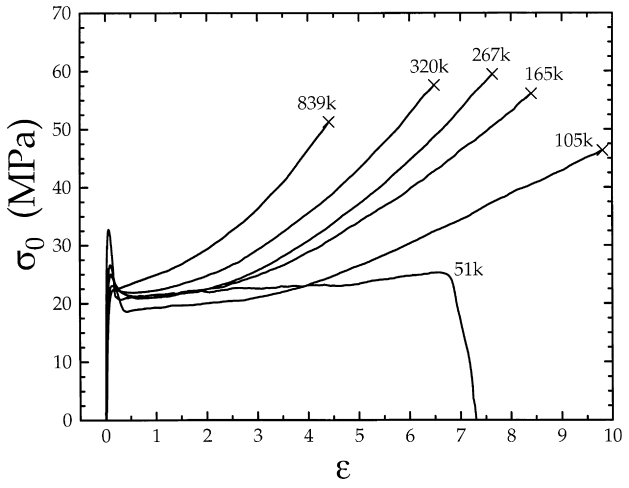

Fig. 9. Stress–strain behavior for the quenched polyethylene series.

3.7. Mechanical properties

In this report, we use engineering stress, σ_0, and nominal strain, ϵ. Yield stress and yield strain, σ_y and ϵ_y, are defined as the values of σ_0 and ϵ at the point where a distinct yield onset is observed, that is, where a peak occurs in the σ_0 vs.ϵ curve. Similarly, the values of stress at break and strain at break, σ_b and ϵ_b, are defined by the point at which the material breaks, except for the case of the quenched 51 kg/mol material which broke in a peculiar fashion. For this material, the values of σ_b and ϵ_b are taken at the point just before formation of a hole in the center of the sample width, near one end of the dog-bone gauge length, which is accompanied by a sharp decrease in stress, to be discussed later. The term tensile strength is avoided here since in some cases it may refer to yield conditions and in others break conditions. Toughness is defined as:

$$\int_{\epsilon=0}^{\epsilon_b} \sigma_0 \, d\epsilon, \tag{8}$$

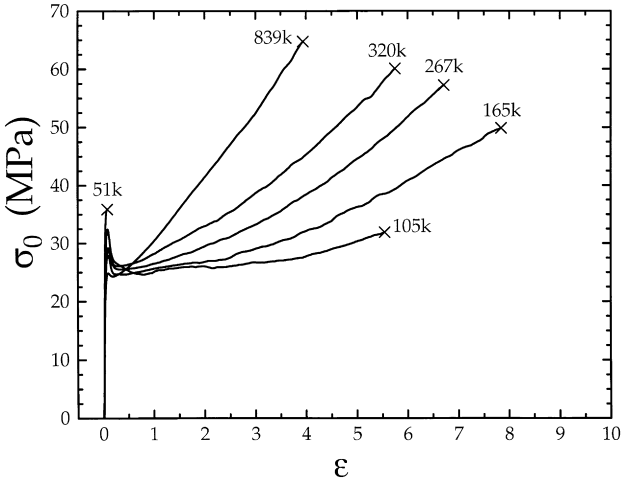

Fig. 10. Stress–strain behavior for the slowly cooled polyethylene series.

which is simply stated as the area under the σ_0 vs. ϵ curve. Although toughness is often reported in units of stress (which is certainly acceptable), we prefer to employ the units of energy per volume. Treating it in this way, leads one to the simple interpretation of toughness as the total energy (or work) required per unit volume to cause failure in the sample [66,67].

The lowest molecular weight polyethylene material (13 kg/mol) could not be tested in the Instron due to extreme brittleness. Merely closing the pneumatic grips caused the sample to crumble. This was the case for both the quenched (79% crystalline) and slowly cooled (83% crystalline) thermal treatments. As a result, the lowest molecular weight sample tested was the 51 kg/mol material. The σ_0–ϵ traces for the quenched and slowly cooled materials for the various molecular weights are presented in Figs. 9 and 10, respectively. Both figures have the same scaling to make differences in the data readily apparent.

For each molecular weight and cooling history, one stress–strain curve that was most representative was plotted in the appropriate figure. (That is, we chose one of the 10 samples that had mechanical properties closest to the statistical averages derived from all 10 specimens. The error bars in Figs. 12 and 13 represent the standard deviations from these averages). In Figs. 9 and 10, breaking points are marked by the symbol (×), except for the quenched 51 kg/mol specimen. This material showed a rather peculiar failure process as mentioned earlier. Firstly, as this ductile material was straining beyond the yield point, the stress level remained fairly constant (no strain hardening). At high strains (≈ 7), a small central hole developed in the dog-bone at one end of the gauge length. As the level of strain continued to increase, this hole grew until finally the sample broke. It is the growth of this hole that leads to the sharp decrease in the stress, rather than a distinct break point. This behavior was observed for all 10 quenched 51 kg/mol specimens.

Unlike the quenched 51 kg/mol material, the slowly cooled form was brittle under the test conditions, and broke shortly after yielding. Hence for a molecular weight of 51 kg/mol, a ductile-to-brittle transition exists somewhere between 70% crystallinity (quenched, ductile material) and 78% (slowly cooled, brittle material). Mandelkern and coworkers have observed [68] a ductile-to-brittle transition in a comparable linear polyethylene ($\bar{M}_w = 54$ kg/mol, $\bar{M}_n = 23$ kg/mol) at a value of 62% crystallinity (these authors varied the thermal history likewise to generate different crystal contents and employed the same drawing conditions). These authors also report that this transition appears to be independent of the type of crystalline superstructure but dependent on crystal content and molecular weight. However, in that study only samples with $\bar{M}_w \leq 120$ kg/mol were probed since higher molecular weights would have required unobtainable crosshead speeds to observe the ductile–brittle transition. They conclude that a small interlamellar thickness is likely responsible for the brittle behavior since small

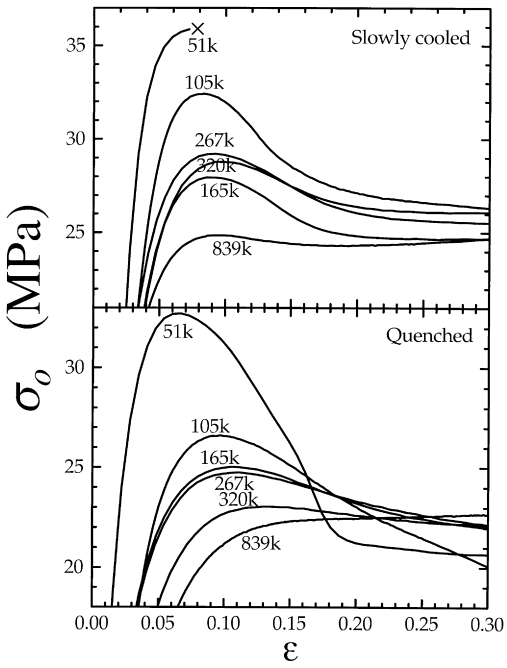

Fig. 11. Stress–strain behavior in the vicinity of yield.

amorphous domains cannot sustain large deformations [68]. Another important factor would be the presence of tie molecules between lamellae. These chains are responsible for carrying a large amount of the stress during the tensile test and the number of tie chains increases with molecular weight [69]. It has also been suggested [70] that the number of ties increases with short-chain branch content. The presence (or lack) of tie chains is one of the critical factors in determining whether a semicrystalline polymer (which is above the glass transition temperature of the amorphous phase) is brittle or ductile. Quenching the 51 kg/mol material may lead to more tie molecules than slowly cooling the same material due to the kinetics of the crystallization process. From the TEM images of Fig. 7, the brittle, slowly cooled 51 kg/mol material in (B) has distinctly thicker lamellae of ≈ 160 Å (and would likely have fewer tie chains) compared to the ≈ 100 Å thick lamellae of the quenched 51 kg/mol material in (C).

Fig. 11 shows an expanded view of the stress–strain curves in the vicinity of yielding for both quenched and slowly cooled treatments. It can be seen from this figure that the yield peak becomes less distinct with increasing molecular weight. The quenched 839 kg/mol polyethylene sample actually does not show a yield maximum, but rather displays a knee and immediately begins to strain harden manifested as the rapid increase in stress level with strain. Kennedy et al. [10] have similarly noted that the yield becomes more diffuse with increasing molecular weight for linear polyethylenes of two types: narrow fractions with $\bar{M}_w/\bar{M}_n$ between 1.14 and 1.43, and zirconocene-catalyzed [71] whole polymers with $\bar{M}_w/\bar{M}_n \approx 2.0$.

The other materials of the series between the 51 kg/mol and quenched 839 kg/mol behaved in a more typical manner. That is, each displayed a distinct yield point, followed by some amount of strain hardening, and a clear

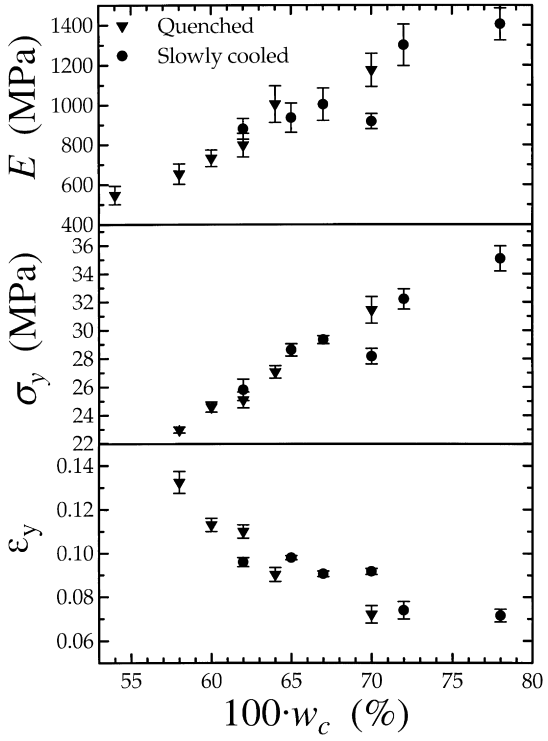

Fig. 12. The dependence of Young's modulus, yield stress, and yield strain on percent crystallinity.

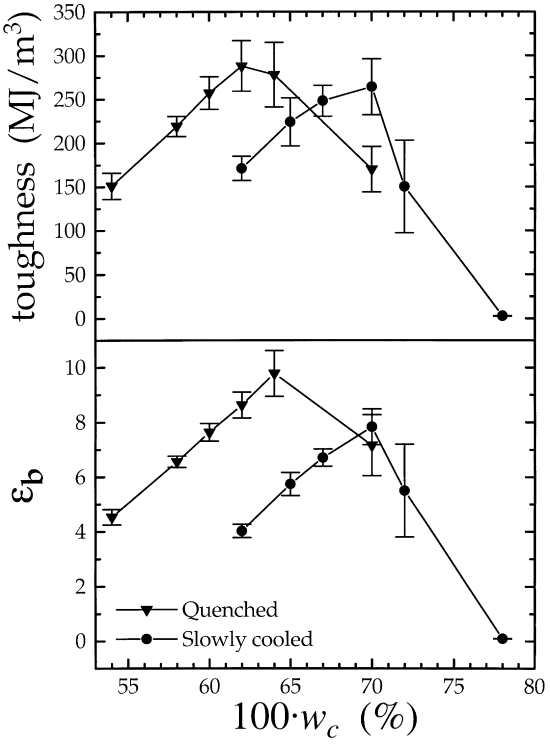

Fig. 13. The dependence of toughness and strain at break on percent crystallinity.

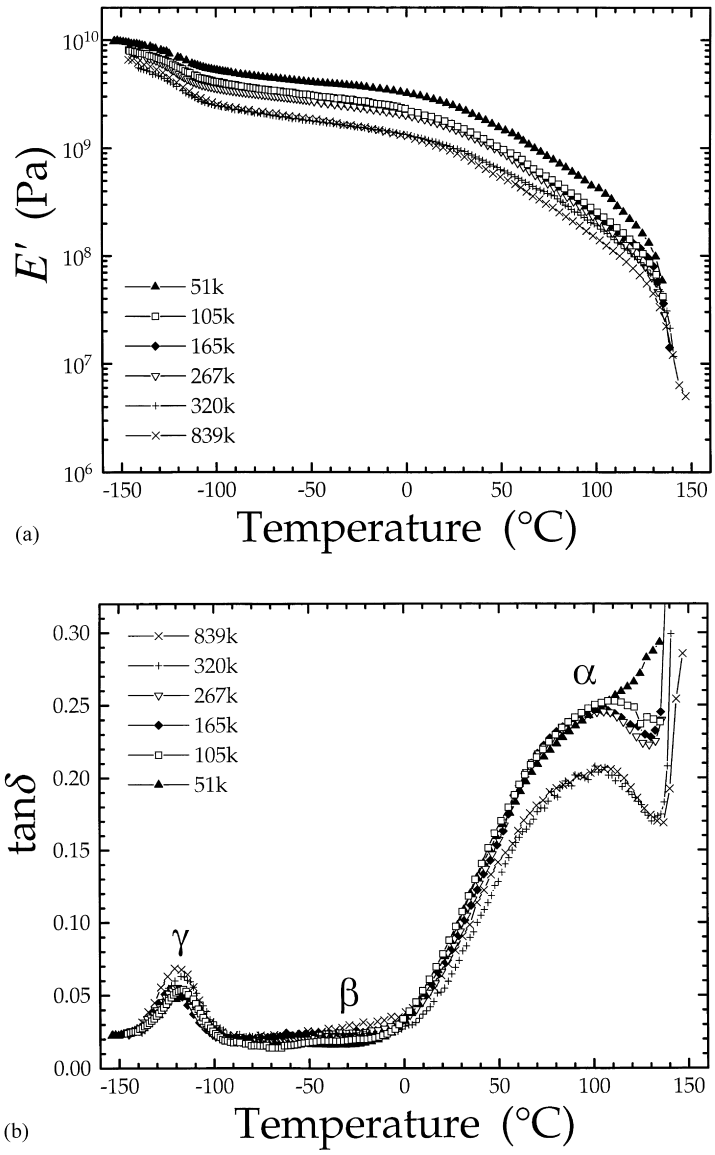

Fig. 14. Dynamic mechanical spectroscopy of the quenched series: (A) storage moduli versus temperature; (B) tan δ versus temperature.

break point. The amount of strain hardening (steepness of the curve in the irrecoverable flow region) increased with molecular weight as previously reported elsewhere [10], presumably because the number of tie molecules increases with molecular weight.

Clearly the stress–strain behavior is dependent on molecular weight and thermal history. Crystal content plays a major role in the small-strain deformation properties (Young's modulus E, ϵ_y and σ_y) in semicrystalline systems and molecular weight and thermal history determine the crystal content. For both thermal histories, the variation of E, ϵ_y and σ_y with crystallinity is illustrated in Fig. 12.

As expected, E increases with crystal content, in fact in a nearly linear fashion. Crist et al. [9] and Janzen and Register [6] have observed a similar relationship between E and density for various polyethylenes. However, at very low values of density, $\rho < 0.92$ g/cm^3 (highly branched molecules), these authors observe a leveling-off in the modulus. The sample set studied here ($\rho > 0.93$ g/cm^3) does not reach a low enough value of density for this to be observed clearly. Popli and Mandelkern [15] also observe a similar lower plateau when they include branched polyethylenes in their analysis of E vs. density.

Not surprisingly, σ_y also increases with crystallinity (Fig. 12) in a nearly linear fashion. Janzen and Register reported [6] a sigmoidal shape to the σ_y-density plot (which covers a broader range of density than the series studied here, particularly in the lower density range). The σ_y data of Crist et al. [9] extend to even lower densities still, but their results would appear to closely follow the sigmoidal shape proposed by Janzen and Register [6]. Thus, our yield stress results and those reported in Refs. [3,9] are in very good general agreement. Also, Kennedy et al. [10] report a linear dependence with an upper plateau for their ranges of

crystallinity. Capaccio and Ward have found [72] that σ_y increases with crystallinity at constant molecular weight for unoriented, melt-crystallized polyethylenes, which is similarly observed in our materials.

There is a decrease in ϵ_y with crystal content (Fig. 12), as expected since it is the amorphous fraction that can undergo the necessary deformation. Janzen and Register noticed a linear relation between density and ϵ_y, which is in agreement with the data presented here [6–8].

In Fig. 12, the data for the slowly cooled samples coincide with the data for the quenched samples. The significance of this is that the small-deformation parameters E, σ_y, and ϵ_y are only dependent on the crystal content, and not on the molecular weight, crystalline superstructure, or other morphological features. This is typical for isotropic semicrystalline systems [6].

Toughness and ϵ_b behave differently with respect to crystal content, as both go through a maximum (Fig. 13). These are large-strain deformation properties, and as such, molecular weight plays a major role in their behavior in addition to crystal content. As seen in Eq. (8), toughness is a function of both σ_o and ϵ. There are many competing processes that cause the observed relationship between toughness and crystal content (or molecular weight). In general, higher molecular weights produce more entanglements per chain, more tie molecules between lamellae, longer relaxation times for reptation [73], and lower crystal contents (for constant thermal treatment) than do lower molecular weights. In polymers of high molecular weight, the many tie molecules allow the sample to carry large stresses, but prevent the sample from deforming to high strains. Also, long relaxation times may prevent high strains (consider the time constant τ_η from the Carreau–Yasuda analysis of the rheological behavior and compare high with low molecular weight; however, it should be noted that τ_η reflects the melt flow behavior and we are currently discussing the solid state). Lower crystal contents would allow greater ultimate strains while carrying less stress. For low molecular weights, shorter relaxation times, fewer entanglements, and fewer tie molecules would drive ϵ_b upward, but higher crystal contents would cause it to decrease and increase the stress. It is the combination of all of these processes that result, for a given deformation rate, in the behavior of toughness and ϵ_b seen in Fig. 13.

3.8. Dynamic mechanical spectroscopy

The mechanical behavior of the series was further examined by DMS. In these experiments, three mechanical relaxations of polyethylene were examined, the α, β, and γ-relaxations. These relaxation processes are described in detail elsewhere [74–86]. Observing all three of these relaxations required scanning from low temperatures (≈−150°C for the frequencies used) to nearly the melting point. Plots of storage modulus (E') and tan $\delta = E''/E'$ (both at 1 Hz) versus temperature appear in Fig. 14(A) and (B) for the quenched series and in Fig. 15(A) and (B) for the slowly cooled series.

First consider the lowest-temperature relaxation process, the γ-relaxation. This relaxation is obvious in the tan δ plots, and its magnitude depends on density, or more appropriately, on amorphous content [74,79]. A closer look at the γ process is given in Fig. 16(A) for the slowly cooled series. There are distinct differences, among the samples, in the magnitudes of the γ-relaxation as seen in the tan δ peaks. This is shown another way in Fig. 16(B), where the peak heights of the γ (and β) relaxations are plotted as functions of the calculated amorphous content. Some additional factor must also play a role in the γ process since the data for the quenched series do not coincide with the data for the slowly cooled series (which would be the case if amorphous content were the only factor). The γ process has been described [79] as a single process occurring exclusively in the amorphous phase of polyethylene and is assigned [80] to the conversion of a "kink" in an otherwise all-trans conformation chain (…$t\,t\,t\,g^+\,t\,g^+\,t\,t\,t$…),[3] to a mirror image of itself (…$t\,t\,t\,g^-\,t\,g^-\,t\,t\,t$…) [80].

The β-relaxations for this series of polyethylenes are very small in magnitude (and for each sample appears as a shoulder to the α-relaxation), and in fact are difficult to discern in some cases. It has been established [74,75,79] that the magnitude of this relaxation increases with branching content. For linear polyethylene, the β-relaxation [74,75,79,87] usually spans a broad temperature window and the magnitude of the relaxation is almost negligible. The same is observed for the materials of this study; this supports our earlier conclusion that the entire series lacks extensive long chain branching. Again referring to Fig. 16(B), the magnitude of the peak in the β region has been plotted as a function of the amorphous content for the slowly cooled series. Despite the very small magnitudes, there appears to be a weak trend here. A dominant effect on the β-relaxation has been observed [87] in designed experiments where the methyl branch content was steadily increased resulting in an increase in the magnitude of the β peak. However, Cooper and McCrum [88] have also observed an apparent β peak due to quenching a linear polyethylene sample from room temperature to liquid-nitrogen temperature before collecting the dynamic mechanical data upon subsequent heating. Data collected on the same material during slowly cooling from room temperature and waiting for thermal equilibrium at each measurement temperature fails to produce this peak in the β region. This second experimental method is considered preferable since the sample is closer to an equilibrium condition, whereas the quenched sample probably has frozen-in thermoelastic stresses [88]. These stresses are perceived to generate the artifact in the β region [88]. Quenching before the experiment also causes an increase the magnitude of the γ-relaxation [88]. The bumps observed in the β region in

[3] t = *trans* conformer, g^+ = *gauche*$^+$, g^- = *gauche*$^-$.

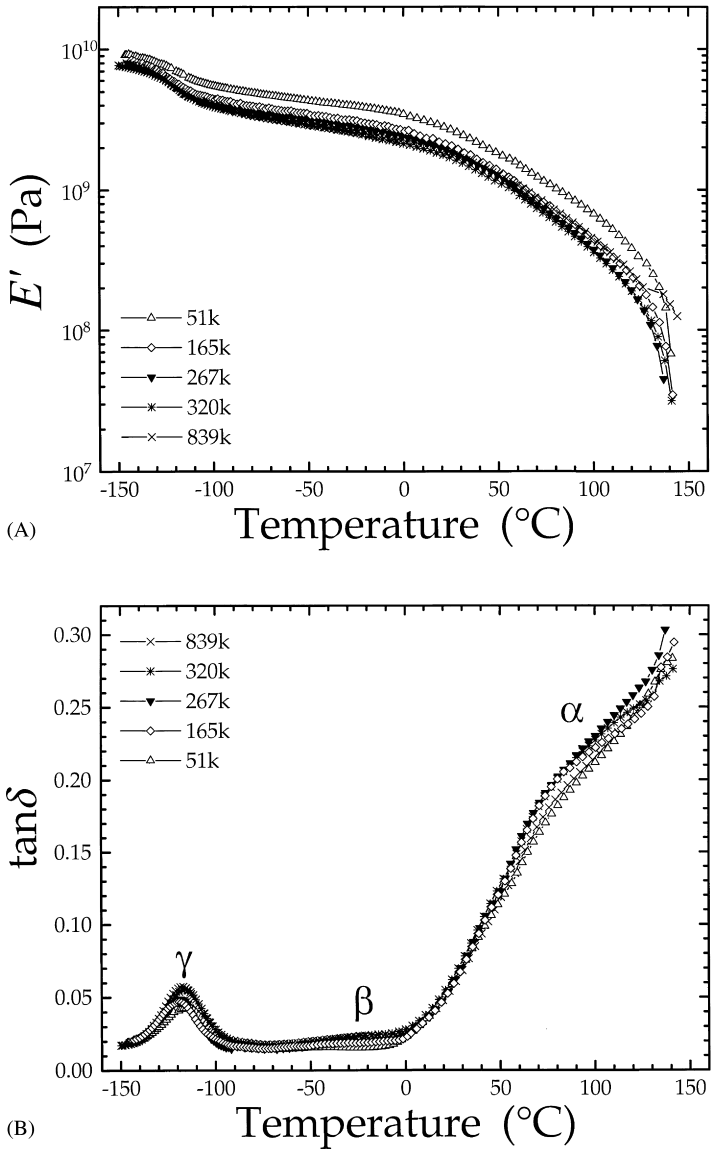

Fig. 15. Dynamic mechanical spectroscopy of the slowly cooled series: (A) storage moduli versus temperature; (B) tan δ versus temperature.

Figs. 14(B) and 15(B) may be due to quenching before the tests and may not be true relaxations. The trend in the peak heights of the β relaxation in Fig. 16 (increasing with increasing molecular weight and hence increasing relaxation time) is in the correct direction to be in accord with this explanation.

In Figs. 14(B) and 15(B), the α relaxations clearly have much higher magnitudes than the other, lower temperature relaxations. The α-relaxation has been assigned [74] to reorientation of molecules within the crystals. A plausible interpretation [80] of this relaxation is the 180° rotational jump followed by translation of the chain through the crystallographic *c*-axis (the chain axis) by one methylene group. This gives rise to a relaxation which can be observed dielectrically or with nuclear magnetic resonance spectroscopy. But the way in which this process would produce a *mechanical* relaxation is not known [74]. In fact the mechanical α-relaxation has been assigned [79] to the amorphous fraction, although it requires the presence of a crystal phase. The mechanical α process is broader and has a longer central relaxation time than the dielectric process [79]. The molecular activity for the mechanical relaxation has been associated with the softening or deformation of the amorphous component and the relaxation time is dependent on lamellar thickness [79]. The characteristics of the mechanical α process are also dependent on molecular orientation [89–91]. The temperature of the α process is also known to increase with lamellar thickness for single crystal mats [92,93], although this trend is not apparent for the data shown in Figs. 14(B) and 15(B). The α-relaxations all begin at ≈ 0°C, and show a broad maximum at nearly the same temperature (≈ 110°C), irrespective of lamellar thickness (which generally increased with molecular weight). There is a marked difference, however, in the shapes of

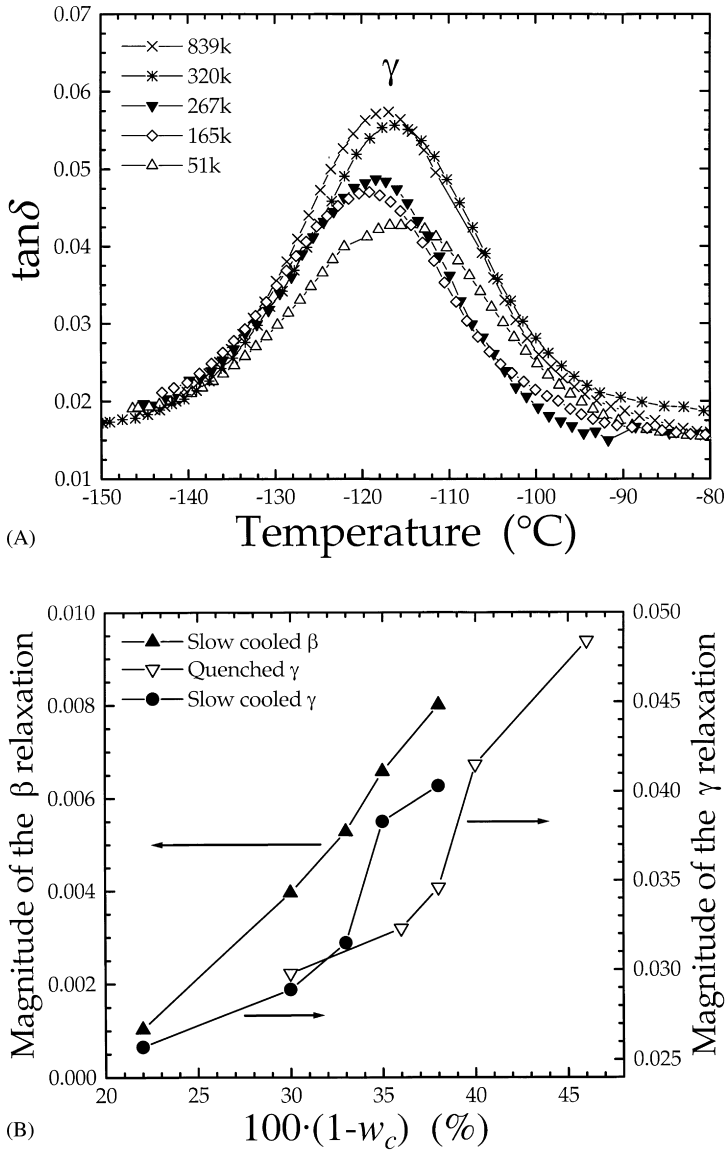

Fig. 16. (A) The loss tangent in the γ-region of the slowly cooled polyethylene series; (B) A plot of the magnitudes of $(\tan\delta)_{max}$ at the γ and β relaxations versus calculated amorphous content.

the α-relaxations when comparing the quenched samples of Fig. 14(B) to the slowly cooled samples of Fig. 15(B). In the quenched materials, there is a distinct α peak. However, in the slowly cooled samples, the α-relaxation appears as more of a shoulder than a peak. The breadths of both are similar. The upturn in the tan δ data at temperatures in excess of 130°C is an artifact due to melting. The data for the slowly cooled samples in the α region most likely represent the properties of the sample prior to the experiment. However, the quenched samples could easily reorganize during the slow heating scan as appropriate temperatures are reached, and hence the properties of these samples could be changing during the experiment [75,89]. (The heating rate through the crystallization window of polyethylene during the DMS scans is between 0.8 and 2.0 K/min.) The α-relaxation peak for the quenched samples therefore may include some component attributable to the molecular motions during any reorganization process that may occur, however a precise fundamental interpretation is impossible [75]. Hence this reorganization process could account for the observed differences in the general shapes of the α-relaxations when comparing the quenched to the slowly cooled polyethylenes.

4. Conclusions

The behavior of this series of metallocene-catalyzed linear polyethylenes is similar to conventional linear polyethylene fractions and whole polymers of narrow molecular weight distribution. This was illustrated by the frequent likening of the metallocene materials to conventional linear

polyethylenes shown in the literature. The main distinction between the metallocene and conventional Ziegler–Natta catalyzed linear polyethylene whole polymers is the more narrow molecular weight distribution obtainable with the former. The molecular weight distribution breadth has a strong effect in the terminal zone, which suggests that significant differences between the two types of polymer would lie in the melt-processing behavior. For the present series of metallocene-catalyzed linear polyethylenes, the following conclusions can be drawn:

The 51 and 320 kg/mol materials both have a melt flow activation energy $E_a \approx 30$ kJ/mol. Values for the other molecular weights are likely to be very nearly the same, and this value implies that the entire series is essentially linear (i.e. no LCB). This conclusion is supported by the dynamic mechanical spectroscopy in which all samples in the series displayed very small magnitude β-relaxations, a characteristic of linear polyethylenes.

For the 51 kg/mol material, a ductile-to-brittle transition exists between 70% (quenched) and 78% (slowly cooled) crystallinity for the drawing conditions employed in this study.

Increasing molecular weight results in a suppression of the yielding point; the magnitude of the "peak" at the yield point decreases with increasing molecular weight. In fact, the quenched form of the highest molecular weight material (839 kg/mol) shows no distinct yield peak in contrast to all lower molecular weights.

As the crystal content increases, both Young's modulus E and the yield stress σ_y increase, while the yield strain ϵ_y decreases, all in a linear fashion for the range of crystallinity probed in this study.

The above three small-deformation mechanical properties E, σ_y, and ϵ_y, are only dependent on the crystal content, and seemingly not on the molecular weight, crystalline superstructure, or other morphological features.

Acknowledgements

The authors extend their gratitude to Mr Steve McCartney for the transmission electron microscopy work, and to Dr David F. Register and Mr Fred J. Burwell for the density measurements. We are grateful to Dr Timothy W. Johnson and Mrs Delores J. Henson for the indispensable SEC determinations of molecular weight distributions and also to Mr Michael J. Hicks for the rheological measurements.

References

[1] Huang J, Rempel GL. Prog Polym Sci 1995;20:459–526.
[2] Hamielec AE, Soares JBP. Prog Polym Sci 1996;21:651–706.
[3] Kaminsky W, Miri M, Sinn H, Woldt R. Makromol Chem, Rapid Commun 1983;4:417.
[4] Reddy SS, Sivaram S. Prog Polym Sci 1995;20:309–67.
[5] Flory PJ. Principles of polymer chemistry. New York: Cornell University Press, 1953.
[6] Janzen J, Register DF. Annu Tech Conf Soc Plast Engng, Indianapolis 1996;2:2190–4.
[7] Janzen J. Polym Engng Sci 1992;32:1242–54.
[8] Janzen J. Polym Engng Sci 1992;32:1255–60.
[9] Crist B, Fisher CJ, Howard PR. Macromolecules 1989;22:1709–18.
[10] Kennedy MA, Peacock AJ, Mandelkern L. Macromolecules 1994;27(19):5297–310.
[11] Kennedy MA, Peacock AJ, Failla MD, Lucas JC, Mandelkern L. Macromolecules 1995;28(5):1407–21.
[12] Peacock AJ, Mandelkern L. J Polym Sci, Part B: Polym Phys 1990;28(11):1917–41.
[13] Failla MD, Lucas JC, Mandelkern L. Macromolecules 1994;27(6):1334–7.
[14] Alamo RG, Chan EKM, Mandelkern L, Voigt-Martin IG. Macromolecules 1992;25(24):6381–94.
[15] Popli R, Mandelkern L. J Polym Sci, Part B: Polym Phys 1987;25(3):441–83.
[16] Rosen SL. Fundamental principles of polymeric materials. 2nd ed.. New York: Wiley, 1993.
[17] Varma-Nair M, Wunderlich B. J Phys Chem Ref Data 1991;20:349–404.
[18] Wunderlich B. Macromolecular physics, Crystal melting, vol. 3. New York: Academic Press, 1980.
[19] Alexander LE. X-ray diffraction methods in polymer science. Malabar, FL: Kreiger, 1969.
[20] Kanig G. Kolliodzeitschrift 1973;251:782–3.
[21] Kanig G. Prog Colloid Polym Sci 1975;57:176–91.
[22] Garbassi F, Gila L, Proto A. Polymer News 1994;19:367–71.
[23] Cox WP, Merz EH. J Polym Sci 1958;28:619–22.
[24] Bird R.B, Armstrong R.C, Hassager O. Dynamics of polymeric liquids, Fluid mechanics. 2nd ed, vol. 1. New York: Wiley, 1987.
[25] Janzen J, Rohlfing DC, Hicks MJ. J Rheol 1999;00:00 (in press).
[26] Pinarbasi A, Liakopoulos A. J Non-Newtonian Fluid Mech 1995;57(2/3):227–41.
[27] Graessley WW. J Chem Phys 1967;47:1942–53.
[28] Graessley WW. Adv Polym Sci 1974;16:1–176.
[29] Berry GC, Fox TG. Adv Polym Sci 1968;5:261–357.
[30] Wilkes GL. J Chem Ed 1981;58:880–92.
[31] Graessley WW, Edwards SF. Polymer 1981;22:1329–34.
[32] Zang Y-H, Carreau PJ. J Appl Polym Sci 1991;42:1965–8.
[33] Porter RS, Knox JP, Johnson JF. Trans Soc Rheol 1968;12:409–19.
[34] Mendelson RA, Bowles WA, Finger FL. J Polym Sci, Polym Phys Ed 1970;8:105–26.
[35] Ngai KL, Plazek DJ. J Polym Sci, Polym Phys Ed 1985;23:2159–80.
[36] Graessley WW. Macromolecules 1982;15:1164–7.
[37] Rohn CL. Analytical polymer rheology. Cincinnati: Hanser Gardner Publications, 1995.
[38] Arnett RL, Thomas CP. J Phys Chem 1980;84:649–52.
[39] Utracki LA, Schlund B. Polym Engng Sci 1987;27(5):367–79.
[40] The JW, Rudin A, Schreiber HP. Plast Rubber Process Appl 1984;4:149.
[41] Vega JF, Santamaría A, Muñoz-Escalona A, Lafuente P. Macromolecules 1998;31:3639–47.
[42] Wasserman SH, Graessley WW. Polym Engng Sci 1996;36:852–61.
[43] Eckstein A, Suhm J, Friedrich C, Maier R-D, Sassmanshausen J, Bochmann M, Mülhaupt R. Macromolecules 1998;31:1335–40.
[44] Whitte WM, Randall JC, Leigh CH. Chem Engng Commun 1983;24:139–46.
[45] Janzen J, Colby RH. J Mol Struct 1999;485–486:569–84.
[46] Graessley WW. J Polym Sci, Polym Phys Ed 1980;18:27–34.
[47] Fetters LJ, Lohse DJ, Richter D, Witten TA, Zirkel A. Macromolecules 1994;27(17):4639–47.
[48] Fetters LJ, Lohse DJ, Colby RH. In: Mark JE, editor. Physical properties of polymers handbook, Woodbury, NY: AIP Press, 1996. p. 335–40.
[49] Carella JM, Graessley WW, Fetters LJ. Macromolecules 1984;17:2775–86.

[50] Wunderlich B. Macromolecular physics, vol. 1. New York: Academic Press, 1973.
[51] Mathot VBF. Calorimetry and thermal analysis of polymers. New York: Hanser, 1994.
[52] Ergoz E, Fatou JG, Mandelkern L. Macromolecules 1972;5:147–57.
[53] Stacy CJ, Arnett RL. J Polym Sci A 1964;2:167–79.
[54] Rault J, Robelin-Souffaché E. J Polym Sci, Polym Phys Ed 1989;27:1349–73.
[55] Hoffman JD, Miller RL. Polymer 1997;38:3151–212.
[56] Bassett DC, Hodge AM. Proc R Soc Lond A 1981;377:25–37.
[57] Bassett DC, Hodge AM, Olley RH. Proc R Soc Lond A 1981;377:39–60.
[58] Bassett DC, Hodge AM. Proc R Soc Lond A 1981;377:61–71.
[59] Keller A. J Polym Sci 1955;17:291–308.
[60] Keith HD, Padden Jr. FJ. Macromolecules 1996;29:7776–86.
[61] Keith HD, Padden Jr. FJ. J Polym Sci 1959;39:123–38.
[62] Keith HD, Padden Jr. FJ. J Polym Sci 1959;39:101–22.
[63] Keller A. J Polym Sci 1959;39:151–73.
[64] Woodward AE. Atlas of polymer morphology. New York: Hanser, 1989.
[65] Voigt-Martin IG, Mandelkern L. J Polym Sci, Polym Phys Ed 1984;22:1901–17.
[66] Wilkes GL. Polymers, mechanical behavior. In: Meyers RA, editor. Encyclopedia of physical science and technology, vol. 11. New York: Academic Press, 1987. p. 61–84.
[67] Ward IM, Hadley DW. Mechanical properties of solid polymers. New York: Wiley, 1993.
[68] Mandelkern L, Smith FL, Failla M, Kennedy MA, Peacock AJ. J Polym Sci, Part B: Polym Phys Ed 1993;31:491–3.
[69] Fink G, Mülhaupt R, Brintzinger HH. Ziegler catalysts. New York: Springer, 1995.
[70] Huang Y-L, Brown N. J Polym Sci, Part B: Polym Phys Ed 1991;29:129–37.
[71] Kaminsky W, Hahnsen H, Külper K, Wöldt R. US Patent 4,542,199, 1985.
[72] Capaccio G, Ward IM. Polymer 1975;16:239–43.
[73] de Gennes P-G. Scaling concepts in polymer physics. New York: Cornell University Press, 1979.
[74] McCrum NG, Read BE, Williams G. Anelastic and dielectric effects in polymeric solids. New York: Wiley, 1967.
[75] McCrum NG. Polyethylene: detailed interpretation of mechanical relaxation in a crystalline polymer. In: Meier DJ, editor. Molecular basis of transitions and relaxations, New York: Gordon and Breach, 1978. p. 167–91.
[76] Takayanagi M. Molecular motions in crystalline polymers. In: Meier DJ, editor. Molecular basis of transitions and relaxations, New York: Gordon and Breach, 1978. p. 117–65.
[77] Hoffman JD, Williams G, Passaglia E. J Polym Sci C 1966;14:173–235.
[78] Gray RW, McCrum NG. J Polym Sci A-2 1969;7:1329–55.
[79] Boyd RH. Polymer 1985;26:323–47.
[80] Boyd RH. Polymer 1985;26:1123–33.
[81] Stehling FC, Mandelkern L. Macromolecules 1970;3:242–52.
[82] Popli R, Glotin M, Mandelkern L. J Polym Sci, Polym Phys Ed 1984;22:407–48.
[83] Rault J. J. Macromol Sci, Rev Macromol Chem Phys C 1997;37:335–87.
[84] Ohta Y, Yasuda H. J Polym Sci, Part B: Polym Phys Ed 1994;32:2241–9.
[85] Schatzki TF. J Polym Sci 1962;57:496.
[86] Schatzki TF. Polym Prepr, Am Chem Soc Div Polym Chem 1965;6:646–51.
[87] Kline DE, Sauer JA, Woodward AE. J Polym Sci 1956;22:455–62.
[88] Cooper JW, McCrum NG. J Mater Sci 1972;7:1221–4.
[89] Zhou H, Wilkes GL. Macromolecules 1997;30:2412–21.
[90] Matthews RG, Ward IM, Capaccio G. J Polym Sci, Part B: Polym Phys 1999;37:51–60.
[91] Buckley CP, McCrum NG. J Polym Sci A-2 1971;9:369–72.
[92] Sinnott KM. J Appl Phys 1966;37:3385.
[93] Takayanagi M, Matsuo T. J Macromol Sci Phys B 1967;1:407.